NANO LETTERS

pubs.acs.org/NanoLett

Letter

Electrically Pumped Polarized Exciton-Polaritons in a Halide Perovskite Microcavity

Tingting Wang,○ Zhihao Zang,○ Yuchen Gao, Chao Lyu, Pingfan Gu, Yige Yao, Kai Peng,* Kenji Watanabe, Takashi Taniguchi, Xiaoze Liu, Yunan Gao,* Wei Bao,* and Yu Ye*

Cite This: *Nano Lett.* 2022, 22, 5175−5181

Read Online

ACCESS | Metrics & More | Article Recommendations | Supporting Information

ABSTRACT: Recently, exciton-polaritons in lead halide perovskite microcavities have been extensively investigated to address striking phenomena such as polariton condensation and quantum emulation. However, a critical step in advancing these findings into practical applications, i.e., realizing electrically pumped perovskite polariton light-emitting devices, has not yet been presented. Here, we devise a new method to combine the device with a microcavity and report the first halide perovskite polariton light-emitting device. Specifically, the device is based on a $CsPbBr_3$ capacitive structure, which can inject the electrons and holes from the same electrode, conducive to the formation of excitons and simultaneously maintaining the high quality of the microcavity. In addition, highly polarized polariton emissions have been demonstrated due to the optical birefringence in the $CsPbBr_3$ microplate. This work paves the way for realizing practical polaritonic devices such as high-speed light-emitting devices for information communications and inversionless electrically pumped lasers based on perovskites.

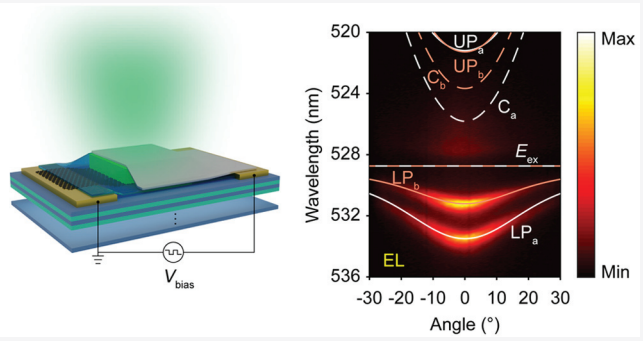

KEYWORDS: *exciton-polariton, electrically pumped, perovskite, microcavity*

Lead halide perovskites provide an ideal platform for optoelectronics due to their outstanding physical properties, including considerable exciton binding energy at room temperature, large oscillator strength, high carrier mobility, low nonradiative recombination rate, tunable band gap, long carrier lifetime, high optical gain, etc.[1−9] Along with the fast-paced developments of photovoltaics and lighting applications, electrically pumped lasers have been a long-sought goal in the research field of perovskite optoelectronics. However, the lasing action usually requires a high enough density of excited carriers for the population inversion of stimulated emission, which has been extremely challenging for the electrical pumping in perovskites so far. This high injection requirement could be significantly relaxed (about 2 orders of magnitude smaller) if the lasing action results from the stimulated scattering of exciton-polaritons.[10] However, the first step, i.e., realizing the electrically pumped exciton-polariton of the perovskite materials, has not yet been presented.

Exciton-polaritons are formed under the strong-coupling regime in semiconductor cavities, where the coupling rate between an exciton and a photon is much faster than the average decay rates of excitons and cavity photons. The hybridization makes the exciton-polaritons possess a quite small effective mass and strong nonlinear interaction strength, leading to the discoveries of fascinating physical phenomena such as polariton condensation and quantum emulation at elevated temperatures in comparison to the ultracold atoms.[11] These physical phenomena have been subsequently discovered in perovskite microcavities, resulting in its renaissance in the past few years:[1,12−25] e.g., polariton lasing and condensation at room temperature,[12,18] Rydberg exciton-polaritons,[19,26] and polariton lattices for quantum emulation and topological physics.[1,20−23] All of the progress shows the great potential of perovskite polaritonics in fundamental research and practical applications. However, no works have shown that the perovskite exciton-polaritons could be electrically pumped so far, even though solution-processed perovskite light-emitting diodes (LEDs) have recently achieved big strides.[27−30] This is because typical LED architectures consisting of thick n-type electron-transport and p-type hole-transport cladding layers sandwiching the perovskite gain medium are not ideal for realizing polariton light-emitting devices: (i) the built-in electric field in the p−i−n structure ionizes excitons,[31] which

Received: March 4, 2022
Revised: June 8, 2022
Published: June 17, 2022

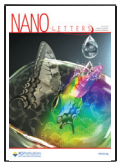

https://doi.org/10.1021/acs.nanolett.2c00906
Nano Lett. 2022, 22, 5175−5181

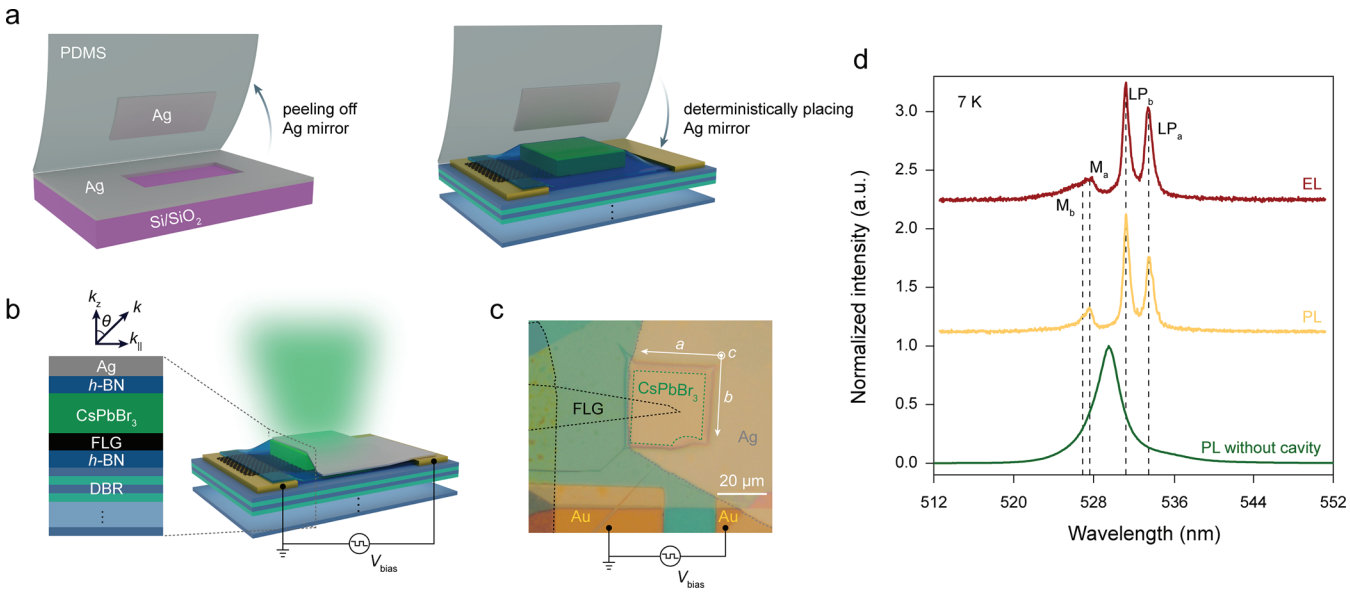

Figure 1. Device schematic and characterization. (a) Schematic of device assembly processes. The Ag mirror is first peeled off from the Ag film previously deposited on a Si/SiO_2 substrate and then deterministically placed on the fabricated device using a dry-transfer method. The specific stacking process is given in Figure S2. (b) Schematic illustration of the final device's structure with a cross-sectional view shown in the inset. (c) Optical microscope image of a typical device. (d) EL (brown trace) and PL (yellow trace) spectra of the $CsPbBr_3$ polariton light-emitting device recorded at 7 K and $\theta = 0°$. A PL (olive green trace) spectrum of the $CsPbBr_3$ microplate on DBR substrate is also provided for comparison. The applied voltage V_{bias} is 20 V with a frequency (f) of 1 MHz for EL measurements, while the optical pump power is 10 μW for PL measurements. The vertical black dashed lines indicate the main emission modes M_a, M_b, LP_a, and LP_b.

hinders the formation of exciton-polaritons; (ii) the thickness of each layer in spin-coated perovskite LEDs is hard to precisely control to form a single-mode emission, desired for exciton-polariton condensation. In addition, the solution process inevitably produces rough interfaces, which leads to poor-quality-factor microcavities. Therefore, it is imperative to devise a new method to assemble perovskite gain materials into architectures that host well-controlled thicknesses, smooth interfaces, high-quality microcavities, and new mechanisms for electron and hole injection in a single device, to realize polariton light-emitting devices. However, it is still challenging.

To address these challenges, we realize an electrically pumped polariton light-emitting device by assembling inorganic perovskite $CsPbBr_3$ microplates with hexagonal boron nitride (h-BN) and few-layer graphite (FLG) in a capacitive structure. Thus, by applying an alternating current (AC) voltage, the electrons and holes can be injected into the $CsPbBr_3$ microplates from the FLG alternately in time but close in space. To form a high-quality microcavity, we develop a new approach to deterministically transfer the silver top mirror. The key feature of this technique is that the materials' interfaces do not contact any organic polymers and solvents during the transfer process, thereby avoiding the introduction of residues in the microcavity and ensuring the smoothness of the interfaces. The transferred silver fragments can be used not only as a mirror[19,24,32,33] but also as an electrode, which can be generalized as a universal technique to meet the needs of any size and position of silver fragments in nano-optoelectronic devices. In this way, the control of the cavity layer's thickness could also be achieved for the cavity resonance condition. The realization of an electrically pumped polariton light-emitting device based on a $CsPbBr_3$ microplate presents a critical step toward ultrafast polariton light emission for communications and electrically pumped inversionless polariton lasers based on perovskites.

To construct a polariton light-emitting device, we assembled a hybrid structure of h-BN/FLG/$CsPbBr_3$/h-BN on a DBR substrate by using an all-dry transfer method.[34,35] Then we used a developed deterministic dry-transfer method (see more details in Methods) to assemble a micrometer-scale silver flake onto the hybrid structure (Figure 1a), acting as a top mirror and an electrode of the light-emitting device at the same time. The bottom DBR mirror is composed of 14.5 pairs of Ta_2O_5/SiO_2 structures, showing a reflectivity of over 99.94% and a stopband ranging from 450 to 615 nm (Figure S1a). Meanwhile, the transferred silver mirror also shows adequate reflectivity. The bare microcavity composed of the bottom DBR and the transferred silver mirror with a 220 nm thick poly(methyl methacrylate) (PMMA) spacer layer shows a resonance at 537 nm with a full width at half-maximum (fwhm) of 0.89 nm and a passive cavity quality factor (Q factor) of ~603 (Figure S1b). In the polariton light-emitting device, the active layer of the $CsPbBr_3$ microplate and the dielectric layers of h-BN are carefully selected and their thickness is accurately measured by atomic force microscopy (AFM) to reach a $5\lambda/2$ cavity mode that resonates with the $CsPbBr_3$ exciton energy (Figure S2 and Table S1). The typical device's optical microscope image (top view) is shown in Figure 1c, with the schematic illustration of the device's structure in Figure 1b. To avert uncoupled exciton emission and an AC capacitive leakage current, we precisely place the top silver flake (marked by the gray dashed line) to completely cover the $CsPbBr_3$ microplate, while minimizing its overlap with the bottom FLG electrode (marked by the black dashed line in Figure 1c). Due to its orthorhombic crystal structure,[36] $CsPbBr_3$ has a mutually orthogonal birefringence effect along the a and b crystalline axes, resulting in two polarization modes when they are coupled to microcavities.[19,20,22]

For the EL measurements, we applied a bipolar square-wave AC voltage (V_{bias}) greater than the turn-on voltage to the top

https://doi.org/10.1021/acs.nanolett.2c00906
Nano Lett. 2022, 22, 5175−5181

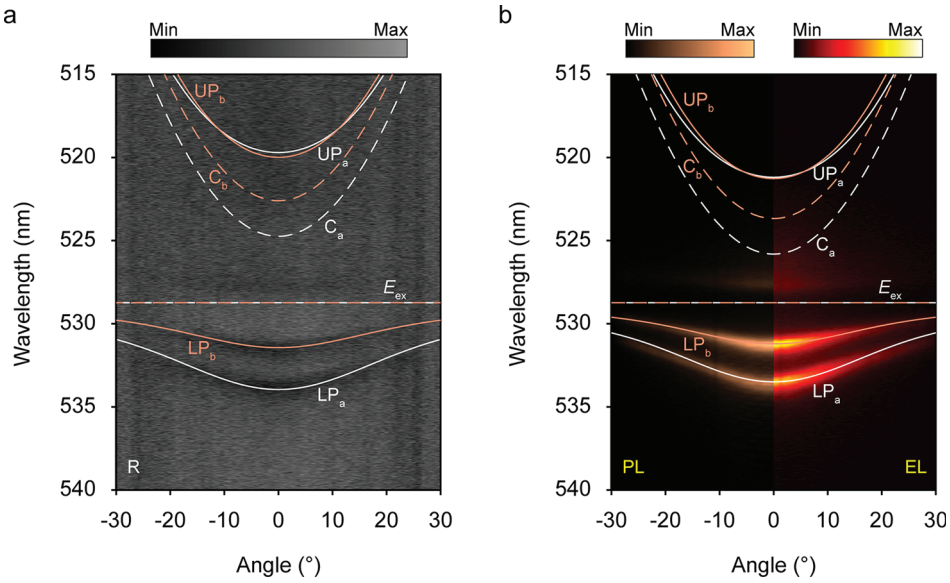

Figure 2. Characterizations of polariton emission dispersions. Angle-resolved reflectivity (a), PL (left panel in (b)), and EL (right panel in (b)) map of the device measured at 7 K. The angle-resolved maps are plotted by interpolation. The horizontal axis represents the angle of the emission relative to the z axis, and the vertical axis is the wavelength. The white and orange solid lines display the theoretical fittings of the upper (UP_a and UP_b) and lower (LP_a and LP_b) polariton dispersions along the a axis and b axis, respectively. The white and orange dashed lines depict the dispersions of uncoupled excitons (E_{ex}) and cavity photon modes (C_a and C_b) obtained from a coupled oscillator model fitted along the a axis and b axis, respectively. The angle-resolved reflectivity and PL maps match with the EL map well.

electrode (silver flake), while the bottom electrode (FLG) was grounded (Figure 1b,c). Due to the long carrier lifetime and the large exciton binding energy of $CsPbBr_3$ at low temperatures, the alternately injected electrons and holes will diffuse in the microplate and form excitons. In order to minimize the heating effect caused by the external field, the photoluminescence (PL) and EL spectra of the device were recorded at 7 K (all temperatures used below are 7 K except where noted otherwise) and $\theta = 0°$ (θ refers to the angle of collected emission direction with relative to the z axis). The PL and EL spectra are consistent with each other, and four emission peaks can be clearly seen (Figure 1d), distinct from the PL emission of the uncoupled $CsPbBr_3$ microplate. The PL of a $CsPbBr_3$ microplate placed on the DBR substrate is also provided for comparison (Figure 1d). In a strong-coupling polariton system, the two peaks at lower energies can be well referred to as the lower polariton branches (LP_a and LP_b), where the subscripts a and b are attributed to the orthogonal birefringence along the two crystal axes, the a axis and b axis, respectively. According to the electromagnetic wave model, it is speculated that the two intermediate branches (M_a and M_b) originate from the significant change in the real part of the refractive index n close to the absorption peak at low temperatures (see more details in Note S1). For the electrically pumped lower polariton branches, LP_a (LP_b) is well resonant with the cavity, with a center at 533.5 nm (531.2 nm), an fwhm of 0.89 nm (0.71 nm), and a Q factor of ∼601 (745). However, due to their large Rabi splitting and strong absorption above the band gap, the upper polariton branches (UP_a and UP_b) cannot be observed here, which is also very common in other inorganic perovskite microcavities.[12,19]

For further confirmation of the light−matter coupling and an illustration of the polariton emission of the $CsPbBr_3$ light-emitting device, we used home-built k-space spectroscopy (Figure S8) to map out the dispersion relationship between wavelength (energy) versus angle (in-plane momentum). In the angle-resolved reflectivity map (Figure 2a), we can clearly distinguish the lower polariton branches, while the upper branches are barely seen. The dispersion curvatures of the LP branches are unambiguously flattened at larger angles, and their resonance frequency shows anticrossing behaviors from parabolic Fabry−Pérot cavity dispersion and flat perovskite exciton energy, firmly indicating that the strong-coupling regime has been reached. Since the focused laser spot reduces the inhomogeneity of the emission, the angle-resolved PL map excited under the nonresonant excitation of the 405 nm continuous-wave (CW) laser (left panel in Figure 2b) shows more pronounced strong-coupling features in comparison to those from the reflectivity map. Due to the inhomogeneity of the structure in the large white light spot (∼30 μm), the polariton modes measured in the reflectivity spectrum have a slight energy shift in comparison to the EL/PL. To better fit the reflectivity dispersions, an effective cavity mode shift was considered to compensate for device inhomogeneity. The intermediate branches caused by the refractive index change are not the main focus of the polariton devices; thus, the dispersion curves of the polariton branches are fitted by the traditional coupled oscillator model (more details on theoretical fitting are given in Note S1). As the temperature increases, the intermediate branches gradually become blurred and eventually disappear above 150 K (Figure S9), which is because the exciton absorption peak becomes weaker and broader and so does the oscillation of n around the absorption peak (Figure S7). By applying a bipolar square voltage with a V_{bias} value of 20 V and an f value of 1 MHz, we obtain strong EL. The angle-resolved EL map (right panel in Figure 2b) matches well with the PL map, which firmly illustrates that the electrically pumped strong-coupling regime has been reached, and the pulsed electrical injection does not cause significant Joule heating. In Figure 2b, using the coupled oscillator model, we can obtain the cavity detuning ($\Delta = E_c - E_{ex}$, where E_c is the cavity photon energy at zero in-plane momentum and E_{ex} is

https://doi.org/10.1021/acs.nanolett.2c00906
Nano Lett. 2022, 22, 5175−5181

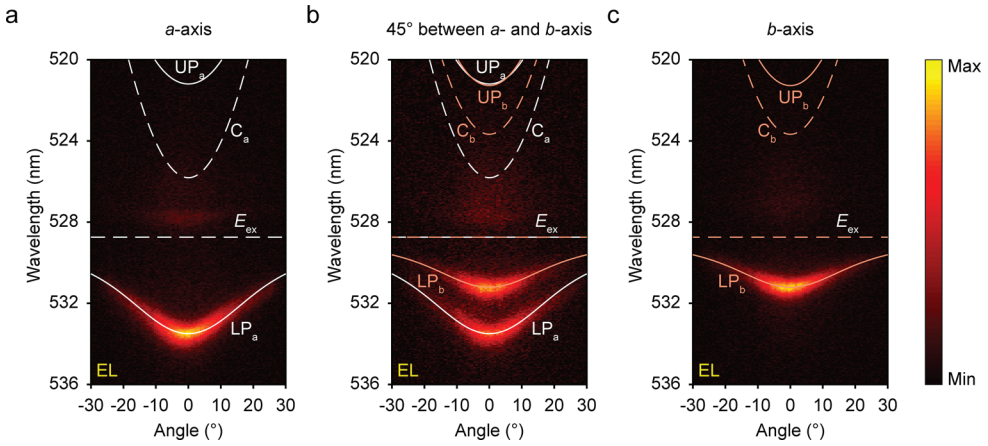

Figure 3. Polarization-resolved EL. Angle-resolved EL maps under a V_{bias} value of 20 V with an f value of 1 MHz, corresponding to the polarization direction along the a axis (a), 45° between the a axis and b axis (b), and b axis (c), respectively. Similarly to Figure 2, the white lines depict the polarization mode along the a axis, while the orange lines depict the orthogonal polarization mode along the b axis.

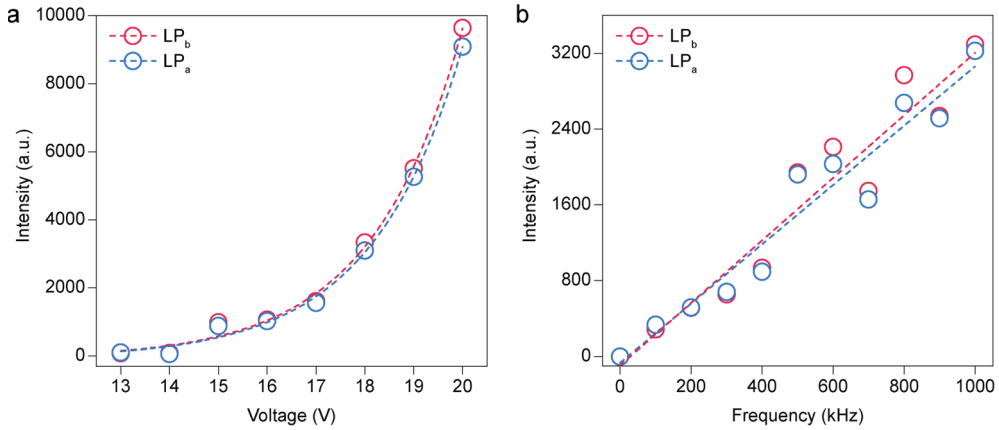

Figure 4. Voltage and frequency dependence of the polariton EL. (a) Voltage-dependent polariton integrated EL intensity under a constant f of 1 MHz. The dashed curves depict the exponential fitting relationship of their respective integrated intensity with voltage. (b) Frequency-dependent polariton integrated EL intensity under a constant V_{bias} of 18 V. The relationship between the integrated intensity and frequency is fitted by a linear function. The acquisition time is 2 s for both (a) and (b).

the exciton energy) between the exciton state and cavity mode along the a axis and b axis, respectively: that is, $\Delta_a = E_{ca} - E_{ex} =$ 13.1 meV and $\Delta_b = E_{cb} - E_{ex} = 22.7$ meV. In addition, we also obtain the Rabi splitting energies, $\hbar\Omega$, between the LP branch and the UP branch along the a axis and b axis, which are 53.28 and 36.66 meV, respectively. These splitting energies are much larger than the corresponding polariton line width, which further justifies that our device is working in the strong-coupling regime. On the basis of the coupled oscillator model, the Hopfield coefficients of each polariton branch can be obtained, which provides the weight of each constituent (Figure S10). Specifically, as the angle increases, the contribution of the excitonic components in the LP branches gradually increases, while the photonic components in the UP branches increase, consistent with a previous report.[11]

Due to the distinct birefringence effect in $CsPbBr_3$ along the a axis and b axis and the single-crystal microplate employed in our devices, it is expected that linearly polarized light sources will be implemented in our light-emitting device. To perform polarization-dependent angle-resolved EL measurements, we sequentially placed a half-wave plate (HWP) and a linear polarizer in the collection light path, and the polarization-dependent signal was collected by rotating the HWP. Figure 3 exhibits the angle-resolved EL maps at three quintessential polarization angles (along the perovskite a axis, 45° between the a axis and b axis, and b axis), superimposed with the theoretical dispersion fittings. When the detection polarization is set along the a (b) axis, only LP_a (LP_b) can be observed, as shown in Figure 3a (Figure 3c). When the detection polarization is set along 45° between the a axis and b axis, both sets of branches can be observed and linearly superimposed (see Figure 3b), indicating they are mutually orthogonal to each other. Optically pumped linearly polarized polaritons in perovskites have previously been reported[19] (see the optically pumped results in our device in Figure S11), and recently polarization has been used as a new degree of freedom to switch between different topological polariton phases.[20] Now, it is realized by electrical means, which not only brings about the linearly polarized light source but also opens up a way to control the polaritons and their polarizations in perovskites electrically.

In our device structure, the pulse voltage can allow a very high injection current density, and the silver flake acts simultaneously as a mirror and an injection electrode so that the injection current will not affect the optical feedback structure. Therefore, we probed the dependence of the

https://doi.org/10.1021/acs.nanolett.2c00906
Nano Lett. 2022, 22, 5175−5181

polariton EL intensity on the excitation voltage and frequency (Figure 4). When the applied voltage frequency, f, is 1 MHz, the EL intensities of the lower polariton branches (LP_a and LP_b) exhibit a threshold behavior with the applied voltage (Figure 4a). The turn-on voltage is about 13 V, and the EL intensity increases exponentially with the applied voltage after the device is turned on. The obvious exponential correlation can be attributed to the increase in the number of injected carriers by the tunneling effect during the bipolar switching (see the band diagrams of the device under applied voltage in different states during a period in Figure S12). In addition, the real-space EL emission image has also been obtained (Figure S13), which extends outward from the source FLG electrode but does not cover the entire $CsPbBr_3$ microplate. This phenomenon is consistent with the working principle (Figure S12), as both electrons and holes are injected through the FLG source electrode at different voltage transients. When the applied bipolar voltage V_{bias} is constant at 18 V, the EL intensities of polariton branches increase linearly with the frequency (Figure 4b). This is because the carrier injection occurs only during the bipolar switching[37−40] (Figure S12) and the EL intensity increases linearly with the number of voltage cycles: namely, the frequency. To avoid ion migration and exciton dissociation in the perovskite under a large applied electric field, the applied voltage is kept at a low level. Note that such a device maintains a stable EL emission over time (Figure S14). It is worth noting that no saturation of EL intensity is observed here, indicating that our structure can realize a strong electrically pumped exciton-polariton polarized light source in the perovskite. To further promote the realization of lasing operation, the structure optimization of the light-emitting layer, improvements in the material performance and the microcavity's Q factor, and a reduction of the turn-on voltage (by tuning the thickness of the h-BN tunneling layer between the perovskite and the silver electrode), etc. are required.

In summary, we have demonstrated an electrically driven $CsPbBr_3$ polariton light-emitting device based on a capacitive structure. A new approach of deterministic dry transfer of the silver flake has also been developed, which could be used as the thin top optical mirror and electrode simultaneously. By fine-tuning the thickness of the cavity, excitons and cavity photons can be strongly coupled to form bright electrically driven polariton emissions. Due to the existence of two polarization modes induced by the birefringence effect of the employed microplate when it is coupled to a microcavity, linearly polarized polariton light sources were realized by electrical means. The powerful technology−material−device combination opens the door to perovskite-based polariton light sources and pushes the electrically pumped polariton perovskite lasers a step closer to reality.

METHODS

Device Fabrication. The silver film was transferred via a deterministic dry transfer method. First, a 30 nm silver film was evaporated on the Si/SiO_2 substrates using electron beam evaporation (EBE) with a deposition rate of 1 Å/s. Then, after the substrate coated with the silver film was fixed, the PDMS stamp was lightly pressed to make it adhere to the silver film. Finally, the PDMS stamp was quickly peeled off, and the silver flakes were transferred from the Si/SiO_2 substrate to the PDMS stamp. Silver flakes of suitable shapes and sizes were then selected for further transfer process by a conventional dry transfer method.

The light-emitting device consists of a bottom DBR, an electrically driven active region (composed of FLG, thin h-BN flakes, and a $CsPbBr_3$ microplate), and a transferred silver film. The bottom DBR is composed of 14.5 pairs of SiO_2/Ta_2O_5 deposited on silicon substrates via ion beam sputtering. The FLG and thin h-BN flakes on PDMS substrates were obtained by mechanical exfoliation from bulk crystals and transferred onto the bottom DBR via a dry-transfer method. The $CsPbBr_3$ microplates were synthesized on mica substrates as described in our previous work[37] and transferred by the PDMS. The thicknesses of each layer in our device were confirmed by AFM (Cypher, Asylum Research) with a tapping mode. Cr (5 nm)/Au (30 nm) electrodes were deposited on the DBR substrates via EBE in advance for electrical measurements.

Optical Spectroscopy Measurements. A schematic diagram of the home-built angle-resolved reflectivity, PL, and EL setup is shown in Figure S8. The device was kept in a liquid helium cryostat (Janis ST-500) for low-temperature measurements, except for absorption. A broad-band white light source (Thorlabs SLS401) was used for angle-resolved reflectivity measurements as well as device imaging. The absorption spectra were measured in a Montana cryostat under a transmission configuration. In terms of angle-resolved PL measurements, the $CsPbBr_3$ light-emitting device was pumped by a CW laser (405 nm). The excitation light beam was focused by an objective (Zeiss Epiplan-Neofluar 50×/0.55 DIC M27). The emitted signals were collected by the same objective and sent into an Andor spectrometer (SR-500i-D2-R) equipped with gratings of 150 and 1200 lines mm^{-1} and a Newton CCD (DU920P-BEX2-DD) of 256 × 1024 pixels.

Electrical Spectroscopy Measurements. Our setup in the Fourier imaging configuration allowed us to access the angle-resolved EL spectra with the help of a pulse generator (Agilent 8114A) providing the AC gate voltage.

ASSOCIATED CONTENT

Supporting Information

The Supporting Information is available free of charge at https://pubs.acs.org/doi/10.1021/acs.nanolett.2c00906.

Characterizations of the bottom DBR and the bare cavity, device fabrication, dispersion fitting, experimental k-space spectroscopy setup, temperature-dependent PL measurements, Hopfield coefficients, polarization-resolved PL, band diagrams, EL emission in real space, and operational stability (PDF)

AUTHOR INFORMATION

Corresponding Authors

Kai Peng − *Electrical & Computer Engineering, University of Nebraska-Lincoln, Lincoln, Nebraska 68588, United States*; Email: kpeng3@unl.edu

Yunan Gao − *State Key Laboratory for Mesoscopic Physics and Frontiers Science Centre for Nano-optoelectronics, School of Physics, Peking University, Beijing 100871, People's Republic of China*; orcid.org/0000-0002-3131-7559; Email: gyn@pku.edu.cn

Wei Bao − *Electrical & Computer Engineering, University of Nebraska-Lincoln, Lincoln, Nebraska 68588, United States*; orcid.org/0000-0003-2974-2625; Email: wbao@unl.edu

https://doi.org/10.1021/acs.nanolett.2c00906
Nano Lett. 2022, 22, 5175−5181

Yu Ye − *State Key Laboratory for Mesoscopic Physics and Frontiers Science Centre for Nano-optoelectronics, School of Physics, Peking University, Beijing 100871, People's Republic of China; Collaborative Innovation Centre of Quantum Matter, Beijing 100871, People's Republic of China; Peking University, Yangtze Delta Institute of Optoelectronics, Nantong 226010 Jiangsu, People's Republic of China;* orcid.org/0000-0001-6046-063X; Email: ye_yu@pku.edu.cn

Authors

Tingting Wang − *State Key Laboratory for Mesoscopic Physics and Frontiers Science Centre for Nano-optoelectronics, School of Physics, Peking University, Beijing 100871, People's Republic of China; Collaborative Innovation Centre of Quantum Matter, Beijing 100871, People's Republic of China*

Zhihao Zang − *State Key Laboratory for Mesoscopic Physics and Frontiers Science Centre for Nano-optoelectronics, School of Physics, Peking University, Beijing 100871, People's Republic of China;* orcid.org/0000-0002-4701-0463

Yuchen Gao − *State Key Laboratory for Mesoscopic Physics and Frontiers Science Centre for Nano-optoelectronics, School of Physics, Peking University, Beijing 100871, People's Republic of China*

Chao Lyu − *State Key Laboratory for Mesoscopic Physics and Frontiers Science Centre for Nano-optoelectronics, School of Physics, Peking University, Beijing 100871, People's Republic of China*

Pingfan Gu − *State Key Laboratory for Mesoscopic Physics and Frontiers Science Centre for Nano-optoelectronics, School of Physics, Peking University, Beijing 100871, People's Republic of China*

Yige Yao − *State Key Laboratory for Mesoscopic Physics and Frontiers Science Centre for Nano-optoelectronics, School of Physics, Peking University, Beijing 100871, People's Republic of China*

Kenji Watanabe − *Research Center for Functional Materials, National Institute for Materials Science, Tsukuba 305-0044, Japan;* orcid.org/0000-0003-3701-8119

Takashi Taniguchi − *International Center for Materials Nanoarchitectonics, National Institute for Materials Science, Tsukuba 305-0044, Japan;* orcid.org/0000-0002-1467-3105

Xiaoze Liu − *School of Physics and Technology, Wuhan University, Wuhan 430072 Hubei, People's Republic of China; Wuhan Institute of Quantum Technology, Wuhan 430206 Hubei, People's Republic of China*

Complete contact information is available at: https://pubs.acs.org/10.1021/acs.nanolett.2c00906

Author Contributions

○T.W. and Z.Z. contributed equally to this work.

Author Contributions

Y.Y. and T.W. conceived the project. T.W. and Z.Z. fabricated the devices and performed the measurements. K.P., W.B., T.W., and Yuchen Gao carried out the theoretical fittings. K.P. and W.B. grew the bottom DBR mirror. K.P., W.B., Yige Yao, and Yunan Gao measured optical absorption spectra. C.L. helped in metal electrode fabrication and the wire bonding process. P.G. helped with the electrical measurements. K.W. and T.T. grew the *h*-BN single crystals. T.W., Z.Z., K.P., W.B., X.L., and Y.Y. performed data analysis and wrote the paper with inputs from all authors. All authors discussed the results, data analysis, and the paper.

Notes

The authors declare no competing financial interest.

■ ACKNOWLEDGMENTS

This work was supported by National Natural Science Foundation of China (No. 61875001) and the National Key R&D Program of China (grant No. 2018YFA0306900). W.B. and K.P. acknowledge support from National Science Foundation (award no. DMR-2143041). X.L. acknowledges support from the National Natural Science Foundation of China (Nos. 62005202 and 12074297), and the National Key R&D Program of China (grant No. 2020YFB2008800). K.W. and T.T. acknowledge support from the Elemental Strategy Initiative conducted by the MEXT, Japan (Grant No. JPMXP0112101001), JSPS KAKENHI (Grant Nos. 19H05790, 20H00354, and 21H05233) and A3 Foresight by JSPS.

■ REFERENCES

(1) Su, R.; Fieramosca, A.; Zhang, Q.; Nguyen, H. S.; Deleporte, E.; Chen, Z.; Sanvitto, D.; Liew, T. C. H.; Xiong, Q. Perovskite Semiconductors for Room-Temperature Exciton-Polaritonics. *Nat. Mater.* **2021**, *20*, 1315−1324.

(2) Blancon, J. C.; Tsai, H.; Nie, W.; Stoumpos, C. C.; Pedesseau, L.; Katan, C.; Kepenekian, M.; Soe, C. M. M.; Appavoo, K.; Sfeir, M. Y.; Tretiak, S.; Ajayan, P. M.; Kanatzidis, M. G.; Even, J.; Crochet, J. J.; Mohite, A. D. Extremely Efficient Internal Exciton Dissociation through Edge States in Layered 2D Perovskites. *Science* **2017**, *355*, 1288−1292.

(3) Zhang, Q.; Su, R.; Liu, X.; Xing, J.; Sum, T. C.; Xiong, Q. High-Quality Whispering-Gallery-Mode Lasing from Cesium Lead Halide Perovskite Nanoplatelets. *Adv. Funct. Mater.* **2016**, *26*, 6238−6245.

(4) Fieramosca, A.; Polimeno, L.; Ardizzone, V.; De Marco, L.; Pugliese, M.; Maiorano, V.; De Giorgi, M.; Dominici, L.; Gigli, G.; Gerace, D.; Ballarini, D.; Sanvitto, D. Two-Dimensional Hybrid Perovskites Sustaining Strong Polariton Interactions at Room Temperature. *Sci. Adv.* **2019**, *5*, No. eaav9967.

(5) Shi, D.; Adinolfi, V.; Comin, R.; Yuan, M.; Alarousu, E.; Buin, A.; Chen, Y.; Hoogland, S.; Rothenberger, A.; Katsiev, K.; Losovyj, Y.; Zhang, X.; Dowben, P. A.; Mohammed, O. F.; Sargent, E. H.; Bakr, O. M. Low Trap-State Density and Long Carrier Diffusion in Organolead Trihalide Perovskite Single Crystals. *Science* **2015**, *347*, 519−522.

(6) Yettapu, G. R.; Talukdar, D.; Sarkar, S.; Swarnkar, A.; Nag, A.; Ghosh, P.; Mandal, P. Terahertz Conductivity within Colloidal $CsPbBr_3$ Perovskite Nanocrystals: Remarkably High Carrier Mobilities and Large Diffusion Lengths. *Nano Lett.* **2016**, *16*, 4838−4848.

(7) Protesescu, L.; Yakunin, S.; Bodnarchuk, M. I.; Krieg, F.; Caputo, R.; Hendon, C. H.; Yang, R. X.; Walsh, A.; Kovalenko, M. V. Nanocrystals of Cesium Lead Halide Perovskites ($CsPbX_3$, X = Cl, Br, and I): Novel Optoelectronic Materials Showing Bright Emission with Wide Color Gamut. *Nano Lett.* **2015**, *15*, 3692−3696.

(8) Yakunin, S.; Protesescu, L.; Krieg, F.; Bodnarchuk, M. I.; Nedelcu, G.; Humer, M.; De Luca, G.; Fiebig, M.; Heiss, W.; Kovalenko, M. V. Low-Threshold Amplified Spontaneous Emission and Lasing from Colloidal Nanocrystals of Caesium Lead Halide Perovskites. *Nat. Commun.* **2015**, *6*, 8056.

(9) Wang, H.; Fang, C.; Luo, H.; Li, D. Recent Progress of the Optoelectronic Properties of 2D Ruddlesden-Popper Perovskites. *J. Semicond.* **2019**, *40*, 041901.

(10) Deng, H.; Weihs, G.; Snoke, D.; Bloch, J.; Yamamoto, Y. Polariton Lasing vs. Photon Lasing in a Semicondyctor Microcavity. *Proc. Natl. Acad. Sci. U. S. A.* **2003**, *100*, 15318−15323.

(11) Deng, H.; Haug, H.; Yamamoto, Y. Exciton-Polariton Bose–Einstein Condensation. *Rev. Mod. Phys.* **2010**, *82*, 1489–1537.
(12) Su, R.; Diederichs, C.; Wang, J.; Liew, T. C. H.; Zhao, J.; Liu, S.; Xu, W.; Chen, Z.; Xiong, Q. Room-Temperature Polariton Lasing in All-Inorganic Perovskite Nanoplatelets. *Nano Lett.* **2017**, *17*, 3982–3988.
(13) Bouteyre, P.; Nguyen, H. S.; Lauret, J. S.; Trippé-Allard, G.; Delport, G.; Lédée, F.; Diab, H.; Belarouci, A.; Seassal, C.; Garrot, D.; Bretenaker, F.; Deleporte, E. Room-Temperature Cavity Polaritons with 3D Hybrid Perovskite: Toward Large-Surface Polaritonic Devices. *ACS Photonics* **2019**, *6*, 1804–1811.
(14) Brehier, A.; Parashkov, R.; Lauret, J. S.; Deleporte, E. Strong Exciton-Photon Coupling in a Microcavity Containing Layered Perovskite Semiconductors. *Appl. Phys. Lett.* **2006**, *89*, 171110.
(15) Nguyen, H. S.; Han, Z.; Abdel-Baki, K.; Lafosse, X.; Amo, A.; Lauret, J. S.; Deleporte, E.; Bouchoule, S.; Bloch, J. Quantum Confinement of Zero-Dimensional Hybrid Organic-Inorganic Polaritons at Room Temperature. *Appl. Phys. Lett.* **2014**, *104*, 081103.
(16) Lanty, G.; Bréhier, A.; Parashkov, R.; Lauret, J. S.; Deleporte, E. Strong Exciton-Photon Coupling at Room Temperature in Microcavities Containing Two-Dimensional Layered Perovskite Compounds. *New J. Phys.* **2008**, *10*, 065007.
(17) Dang, N. H. M.; Gerace, D.; Drouard, E.; Trippé-Allard, G.; Lédeé, F.; Mazurczyk, R.; Deleporte, E.; Seassal, C.; Nguyen, H. S. Tailoring Dispersion of Room-Temperature Exciton-Polaritons with Perovskite-Based Subwavelength Metasurfaces. *Nano Lett.* **2020**, *20*, 2113–2119.
(18) Su, R.; Wang, J.; Zhao, J.; Xing, J.; Zhao, W.; Diederichs, C.; Liew, T. C. H.; Xiong, Q. Room Temperature Long-Range Coherent Exciton Polariton Condensate Flow in Lead Halide Perovskites. *Sci. Adv.* **2018**, *4*, No. eaau0244.
(19) Bao, W.; Liu, X.; Xue, F.; Zheng, F.; Tao, R.; Wang, S.; Xia, Y.; Zhao, M.; Kim, J.; Yang, S.; Li, Q.; Wang, Y.; Wang, Y.; Wang, L. W.; MacDonald, A. H.; Zhang, X. Observation of Rydberg Exciton Polaritons and Their Condensate in a Perovskite Cavity. *Proc. Natl. Acad. Sci. U. S. A.* **2019**, *116*, 20274–20279.
(20) Su, R.; Ghosh, S.; Liew, T. C. H.; Xiong, Q. Optical Switching of Topological Phase in a Perovskite Polariton Lattice. *Sci. Adv.* **2021**, *7*, No. eabf8049.
(21) Su, R.; Ghosh, S.; Wang, J.; Liu, S.; Diederichs, C.; Liew, T. C. H.; Xiong, Q. Observation of Exciton Polariton Condensation in a Perovskite Lattice at Room Temperature. *Nat. Phys.* **2020**, *16*, 301–306.
(22) Spencer, M. S.; Fu, Y.; Schlaus, A. P.; Hwang, D.; Dai, Y.; Smith, M. D.; Gamelin, D. R.; Zhu, X.-Y. Spin-Orbit–Coupled Exciton-Polariton Condensates in Lead Halide Perovskites. *Sci. Adv.* **2021**, *7*, No. eabj7667.
(23) Li, Y.; Ma, X.; Zhai, X.; Gao, M.; Dai, H.; Schumacher, S.; Gao, T. Manipulate Polariton Condensates by Rashba-Dresselhaus Effect at Room Temperature. **2021**, arXiv:2108.02057 [cond-mat.quant-gas]. DOI: 10.48550/arXiv.2108.02057 (accessed June 8th, 2022).
(24) Polimeno, L.; Lerario, G.; De Giorgi, M.; De Marco, L.; Dominici, L.; Todisco, F.; Coriolano, A.; Ardizzone, V.; Pugliese, M.; Prontera, C. T.; Maiorano, V.; Moliterni, A.; Giannini, C.; Olieric, V.; Gigli, G.; Ballarini, D.; Xiong, Q.; Fieramosca, A.; Solnyshkov, D. D.; Malpuech, G.; Sanvitto, D. Tuning of the Berry Curvature in 2D Perovskite Polaritons. *Nat. Nanotechnol.* **2021**, *16*, 1349–1354.
(25) Wang, J.; Su, R.; Xing, J.; Bao, D.; Diederichs, C.; Liu, S.; Liew, T. C. H.; Chen, Z.; Xiong, Q. Room Temperature Coherently Coupled Exciton-Polaritons in Two-Dimensional Organic-Inorganic Perovskite. *ACS Nano* **2018**, *12*, 8382–8389.
(26) Gu, J.; Walther, V.; Waldecker, L.; Rhodes, D.; Raja, A.; Hone, J. C.; Heinz, T. F.; Kéna-Cohen, S.; Pohl, T.; Menon, V. M. Enhanced Nonlinear Interaction of Polaritons via Excitonic Rydberg States in Monolayer WSe_2. *Nat. Commun.* **2021**, *12*, 2269.
(27) Van Le, Q.; Jang, H. W.; Kim, S. Y. Recent Advances toward High-Efficiency Halide Perovskite Light-Emitting Diodes: Review and Perspective. *Small Methods* **2018**, *2*, 1700419.
(28) Lin, K.; Xing, J.; Quan, L. N.; de Arquer, F. P. G.; Gong, X.; Lu, J.; Xie, L.; Zhao, W.; Zhang, D.; Yan, C.; Li, W.; Liu, X.; Lu, Y.; Kirman, J.; Sargent, E. H.; Xiong, Q.; Wei, Z. Perovskite Light-Emitting Diodes with External Quantum Efficiency Exceeding 20%. *Nature* **2018**, *562*, 245–248.
(29) Hassan, Y.; Park, J. H.; Crawford, M. L.; Sadhanala, A.; Lee, J.; Sadighian, J. C.; Mosconi, E.; Shivanna, R.; Radicchi, E.; Jeong, M.; Yang, C.; Choi, H.; Park, S. H.; Song, M. H.; De Angelis, F.; Wong, C. Y.; Friend, R. H.; Lee, B. R.; Snaith, H. J. Ligand-Engineered Bandgap Stability in Mixed-Halide Perovskite LEDs. *Nature* **2021**, *591*, 72–77.
(30) Kim, Y. H.; Kim, S.; Kakekhani, A.; Park, J.; Park, J.; Lee, Y. H.; Xu, H.; Nagane, S.; Wexler, R. B.; Kim, D. H.; Jo, S. H.; Martínez-Sarti, L.; Tan, P.; Sadhanala, A.; Park, G. S.; Kim, Y. W.; Hu, B.; Bolink, H. J.; Yoo, S.; Friend, R. H.; Rappe, A. M.; Lee, T. W. Comprehensive Defect Suppression in Perovskite Nanocrystals for High-Efficiency Light-Emitting Diodes. *Nat. Photonics* **2021**, *15*, 148–155.
(31) D'Innocenzo, V.; Grancini, G.; Alcocer, M. J. P.; Kandada, A. R. S.; Stranks, S. D.; Lee, M. M.; Lanzani, G.; Snaith, H. J.; Petrozza, A. Excitons versus Free Charges in Organo-Lead Tri-Halide Perovskites. *Nat. Commun.* **2014**, *5*, 3586.
(32) Zhang, L.; Wu, F.; Hou, S.; Zhang, Z.; Chou, Y. H.; Watanabe, K.; Taniguchi, T.; Forrest, S. R.; Deng, H. Van Der Waals Heterostructure Polaritons with Moiré-Induced Nonlinearity. *Nature* **2021**, *591*, 61–65.
(33) Gu, J.; Chakraborty, B.; Khatoniar, M.; Menon, V. M. A Room-Temperature Polariton Light-Emitting Diode Based on Monolayer WS2. *Nat. Nanotechnol.* **2019**, *14*, 1024–1028.
(34) Meitl, M. A.; Zhu, Z.; Kumar, V.; Lee, K. J. A. E.; Feng, X. U. E.; Huang, Y. Y.; Adesida, I.; Nuzzo, R. G.; Rogers, J. A. Transfer Printing by Kinetic Control of Adhesion to an Elastomeric Stamp. *Nat. Mater.* **2006**, *5*, 33–38.
(35) Kim, S.; Wu, J.; Carlson, A.; Hun, S.; Kovalsky, A.; Glass, P.; Liu, Z.; Ahmed, N.; et al. Microstructured Elastomeric Surfaces with Reversible Adhesion and Examples of Their Use in Deterministic Assembly by Transfer Printing. *Proc. Natl. Acad. Sci. U. S. A.* **2010**, *107*, 17095–17100.
(36) Rodová, M.; Brožek, J.; Knížek, K.; Nitsch, K. Phase Transitions in Ternary Caesium Lead Bromide. *J. Therm. Anal. Calorim.* **2003**, *71*, 667–673.
(37) Cheng, X.; Zang, Z.; Yuan, K.; Wang, T.; Watanabe, K.; Taniguchi, T.; Dai, L.; Ye, Y. A Hybrid Structure Light-Emitting Device Based on a $CsPbBr_3$ Nanoplate and Two-Dimensional Materials. *Appl. Phys. Lett.* **2020**, *116*, 263103.
(38) Cho, S. H.; Sung, J.; Hwang, I.; Kim, R. H.; Choi, Y. S.; Jo, S. S.; Lee, T. W.; Park, C. High Performance AC Electroluminescence from Colloidal Quantum Dot Hybrids. *Adv. Mater.* **2012**, *24*, 4540–4546.
(39) Lien, D. H.; Amani, M.; Desai, S. B.; Ahn, G. H.; Han, K.; He, J. H.; Ager, J. W.; Wu, M. C.; Javey, A. Large-Area and Bright Pulsed Electroluminescence in Monolayer Semiconductors. *Nat. Commun.* **2018**, *9*, 1229.
(40) Zhao, Y.; Wang, V.; Lien, D. H.; Javey, A. A Generic Electroluminescent Device for Emission from Infrared to Ultraviolet Wavelengths. *Nat. Electron.* **2020**, *3*, 612–621.

https://doi.org/10.1021/acs.nanolett.2c00906
Nano Lett. 2022, 22, 5175–5181